JOURNAL OF THERMOPHYSICS AND HEAT TRANSFER
Vol. 10, No. 3, July–September 1996

Heat Transfer Inside and Downstream of Cavities Using Transient Liquid Crystal Method

Srinath V. Ekkad* and Je-Chin Han†
Texas A&M University, College Station, Texas 77843

Local heat transfer coefficient distributions are investigated inside and downstream of various cavities on a flat surface. The effect of cavity size, depth, and shape are studied using a transient liquid crystal image method. Liquid crystals are sprayed on the test surface and a hot mainstream is imposed, suddenly causing a color change. The time of color change is obtained using an image processing system. An increase in cavity size for the same depth increases heat transfer coefficients on the test surface. An increase in cavity depth increases downstream heat transfer coefficients. Five cavity shapes are studied to compare local heat transfer behavior for the effect of various shapes.

Nomenclature

c_p = specific heat of test surface material
D = hydraulic diameter of cavity
d = cavity depth
h = local convection heat transfer coefficient with cavity
h_0 = local convection heat transfer coefficient without cavity
k = thermal conductivity of test surface material
Re_x = Reynolds number based on axial distance, $\rho Ux/\mu$
Re_θ = momentum thickness Reynolds number, $\rho U\theta/\mu$
T = temperature
Tu = freestream turbulence intensity
t = time of liquid crystal color change
U = mainstream velocity
x = axial distance along the mainstream
z = spanwise distance
α = thermal diffusivity of test surface material
Δ = temperature step
δ = boundary-layer thickness
δ^* = displacement thickness
θ = momentum thickness of the boundary layer
μ = fluid dynamic viscosity
ρ = fluid density
τ = time step

Introduction

MODERN gas-turbine engine components use thermal barrier coatings (TBC) to protect the metal surfaces from high-temperature gases in the postcombustion stage. Because of thermal stresses, erosion, and corrosion, the coating surface chips off and exposes the inner metal to the high-temperature gases. The chipping of the TBC is called spallation. Spallation is a serious problem that causes loss of protection to the metal surface from high-temperature gases and enhances local heat transfer coefficients. This enhancement of heat transfer on the surface because of spallation could be detrimental to the overall life and efficiency of the gas-turbine components. Since in the real turbine, it is difficult to specify the geometry of the spallation, several sizes, depths, and shapes are tested in this study to understand the heat transfer enhancement caused by the spalding.

This study focuses on the heat transfer augmentation caused by the TBC spallation. The real TBC coating surface and its spallation are not used in this study. Instead, the TBC spallation is modeled by a cavity on a smooth flat surface. Various sizes, depths, and shapes of cavities are tested on a Plexiglas® test surface to obtain the heat transfer augmentation.

Flow and heat transfer in rectangular cavities were studied.[1-4] Cavities installed in wind-tunnel walls where the cavity opened to a well-developed, zero-pressure gradient flow over an otherwise smooth surface were studied.[1-3] Metzger et al.[4] studied a narrow slot-type channel where one bounding wall contained a transverse rectangular cavity. In the present study, the cavity is part of an otherwise smooth wall. The cavities are of different shapes rather than the rectangular ones studied earlier. More detailed heat transfer measurements in and around the cavity surface are presented compared with other studies.

The present study employs a transient test on a liquid crystal-coated test surface. Ireland and Jones[5] developed a transient liquid crystal technique to measure local heat transfer coefficients in blade cooling geometries. Clifford et al.[6] and Metzger and Larson[7] used phase-change paints instead of liquid crystals for transient heat transfer coefficient measurements. Hippensteele et al.[8] used liquid crystal images and a steady-state technique to measure local heat transfer coefficients on curved surfaces. Camci et al.[9] presented a hue-capturing technique for measuring heat transfer coefficients, using both steady-state and transient methods and a liquid crystal coating. Baughn and Yan[10] and Hippensteele and Poinsatte[11] used a transient technique with a liquid crystal coating on heated ducts. Camci et al.[12] and Wang et al.[13] developed new methods to process liquid crystal color change during a transient test. Ekkad and Han[14] presented a transient liquid crystal technique to measure local heat transfer coefficients near a sharp 180-deg turn of a two-pass smooth square channel.

The present study uses the same technique used by Ekkad and Han.[14] The surface is coated with a thin liquid crystal coating and suddenly exposed to a hot mainstream. The liquid crystal coating changes color and an image processing system measures the time of color change. This technique has many advantages over the classical thermocouple technique. High resolution data can be obtained for complex geometries.

Test Apparatus

Figure 1 presents the experimental setup. The image processing system consists of an RGB camera, a color monitor,

Received Sept. 14, 1995; revision received Jan. 23, 1996; accepted for publication Jan. 24, 1996.

*Research Associate, Department of Mechanical Engineering.
†HTRI Professor, Department of Mechanical Engineering. Associate Fellow AIAA.

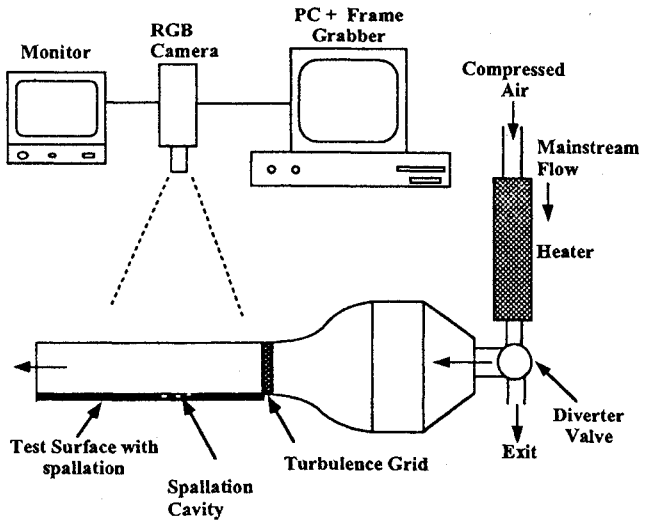

Fig. 1 Illustration of the experimental setup.

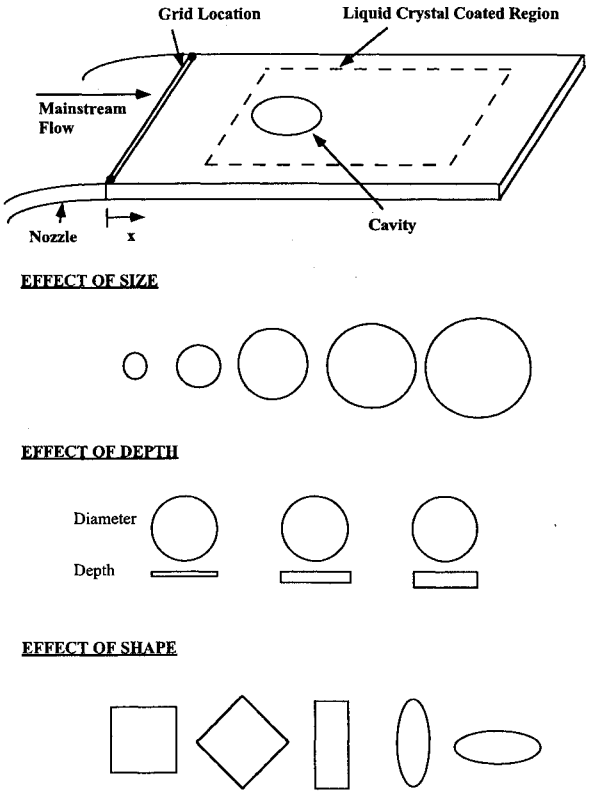

Fig. 2 Test plate configuration and spallation geometries.

and a personal computer with a color frame grabber board. The frame grabber board analyzes the color change using commercially available software that analyzes the surface frame-by-frame for time of liquid crystal color change from colorless to green. Figure 1 also shows the flow circuit. The flow circuit consists of a compressor-based air supply. Compressed air passes through an orifice meter that measures the flow rate and then through an in-line heater. The air heater heats the mainstream to a required temperature. A ball diverter valve routes the hot air away from the test section. The transient test is initiated when the valve is flipped and the hot air is let into the test duct. A thermocouple, connected to a strip chart recorder, measures the varying mainstream temperature during the transient test.

Figure 1 also shows the test tunnel. The test plate is a piece of 1.27-cm-thick, black Plexiglas. The test section is a 10.16-$\times$ 15.24-cm-rectangular and 44.5-cm-long Plexiglas tunnel. A nozzle is placed before the rectangular duct for making flow uniform. A grid placed between the nozzle and the duct generates higher freestream turbulence. The grid is a biplanar square-bar grid with 50% porosity at the nozzle exit. A smooth plate and 12 plates with cavities are fabricated for testing. Upstream edges of each cavity are 21.6 cm from the turbulence grid.

Figure 2 shows the cavity geometries. Five circular shapes of 1.27, 2.54, 3.81, 5.08, and 6.35 cm diameters, with a similar depth of 0.51 cm, are tested for the effect of cavity size. Three different depths of 0.254, 0.51, and 0.76 cm are tested for a circular cavity of diameter 3.81 cm for the effect of depth. Five different shapes: square, diamond, rectangle, vertical ellipse, and a horizontal ellipse, with the same 0.51 cm depth, are tested for cavity shape. Table 1 summarizes the geometries studied.

Theory

The liquid crystal coating is first calibrated to obtain the actual appearance of green under laboratory light conditions. A copper bar is coated with liquid crystals and heated. Time-of-color change on the copper bar is measured and the temperature of the copper bar is monitored on a chart recorder. Time is correlated on the temperature curve to obtain the actual temperature of the appearance of green. Color change temperature is different for different liquid crystal formulations.

Local heat transfer coefficient h over a Plexiglas surface coated with liquid crystals can be obtained by using a one-dimensional semi-infinite solid assumption for the test surface. Solving the one-dimensional transient conduction equation with prescribed initial and boundary conditions, one obtains the nondimensional temperature at the convective boundary surface:

$$(T_w - T_i)/(T_m - T_i) = 1 - \exp(h^2\alpha t/k^2)\operatorname{erfc}(h\sqrt{\alpha t}/k) \quad (1)$$

Knowing the initial temperature T_i of the test surface and the mainstream temperature T_m, and measuring the time t at which the liquid color change appears on the test surface, the coefficient h can be calculated from Eq. (1). The duration of the testing time is kept small so that the semi-infinite solid assumption is valid and the mainstream is heated to a temperature that produces color change times between 20–80 s. Lateral conduction effects were determined to be small for this type of solution.[15]

A chart recorder measures the gradual change of the mainstream temperature during the transient test. Since the mainstream temperature now depends on time, the solution has to include the gradual change of the mainstream temperature. A time history of T_m is reproduced as a series of step functions. Figure 3 illustrates a time-temperature history during the tests. The smooth curve displays the actual temperature behavior. Step changes are also shown in the figure. Using Duhamel's superposition theorem, the solution in Eq. (1) can be represented in terms of the changing mainstream as

$$T_w - T_i = \sum_{j=1}^{N} \left\{ 1 - \exp\left[\frac{h^2\alpha(t - \tau_j)}{k^2}\right] \times \operatorname{erfc}\left[\frac{h\sqrt{\alpha(t - \tau_j)}}{k}\right] \right\} (\Delta T_m) \quad (2)$$

where ΔT_m and τ_j are the mainstream temperature and time steps from the chart recorder output. Equation (2) is solved to obtain the local heat transfer coefficient at every point on the measured region (55 $\times$ 70 points).

Table 1 Various cavity configurations presented in this study

Shape	Size, cm	Depth, cm
Circle	Diameters = 1.27, 2.54, 3.81, 5.08, 6.35	0.51
Circle	Diameter = 3.08	0.254, 0.51, 0.76
Square	Side = 3.81	0.51
Diamond	Side = 3.81	0.51
Rectangle (spanwise)	Sides = 5.08 × 1.91	0.51
Ellipse (spanwise)	Axes = 5.08 × 1.91	0.51
Ellipse (streamwise)	Axes = 1.91 × 5.08	0.51

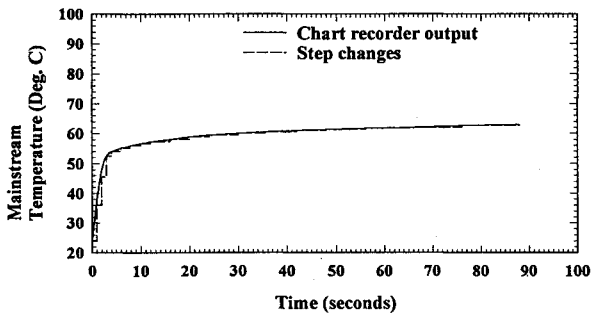

Fig. 3 Mainstream temperature dependence on time.

Procedure

The test surface is sprayed with a thin coating of commercially available encapsulated liquid crystal (Hallcrest, type BM/R32C5W/C17-10). A primary color display of the liquid crystals is from an initial colorless to red, green, and blue, and then colorless again. A color-to-temperature calibration produced color change temperatures to red, green, and blue at 31.6, 32.7, and 37.2°C, respectively. The coating is a light spray of thickness in the order of 1–5 μm. Ireland and Jones[16] showed the response time of the liquid crystals to be only a few milliseconds. Duration of the transient test is much larger than the response time of the liquid crystals.

A compressor supplies the mainstream air. Air passes through an in-line heater that heats the air to a steady temperature. Once the air temperature is steady, a valve is flipped and the air is sent over the test surface, causing the liquid crystals to change color. Time of color change to green is measured at every location and the heat transfer coefficient is calculated using Eq. (2). Experimental uncertainty in calculating h, estimated by the method of Kline and McClintock,[17] is about ±6.5%. Uncertainties in the measurement of the time of color change t (±3.4%), T_m (±1.5%), color change temperature T_w (±0.8%), and the wall material properties α and k (±3.0%), are included in the calculation of the overall uncertainty in the measurement of h.

Results and Discussion

The mainstream velocity for all of the tests was maintained at 7.4 m/s. A mainstream Reynolds number based on the location of the upstream edge of the cavity from the turbulence grid was obtained to be 1×10^5. Mainstream flow was tested for uniformity by measuring velocity profiles parallel and normal to the test plate. Turbulent boundary-layer velocity was measured at the upstream edge of the cavity location. Boundary-layer thickness δ was 1.02 cm, δ^* was 0.127 cm, θ was 0.096 cm, and Re_θ was obtained to be 447. Centerline free-stream turbulence intensity at the upstream of the cavity was measured as 8.5%, using a single hot wire. The corresponding streamwise dissipation length scale was estimated to be 0.5 cm. A four-channel TSI IFA 100 constant temperature anemometer (CTA) was connected to a personal computer through a data translation DT2831-G A/D board to digitize the hot-wire signal.

The results are presented as a ratio of heat transfer coefficients. The coefficient h is normalized with h_0 to obtain the local heat transfer enhancement because of the cavity. This ratio (h/h_0) is presented for the effect of cavity size, depth, and shape.

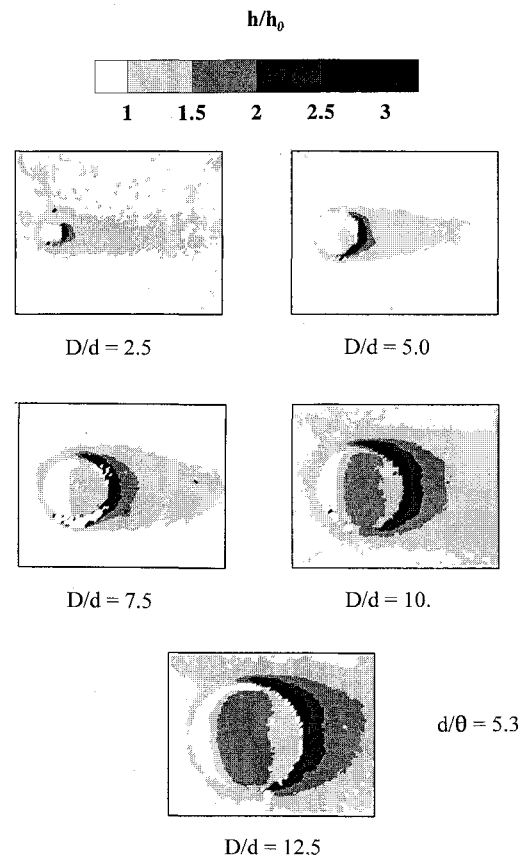

Fig. 4 Effect of cavity size on local h/h_0 distributions.

Effect of Cavity Size

Effect of size D is tested on a circular cavity of increasing diameters of 1.27, 2.54, 3.81, 5.08, and 6.35 cm. The depth d is 0.51 cm for all of the cavity sizes. The d/θ value is 5.3 for all of the sizes. Figure 4 presents the local heat transfer coefficient ratio distributions for all circular cavity sizes. Effect of the cavity size on heat transfer coefficient augmentation is typically one diameter downstream of the cavity. With increasing size, the heat transfer enhancement downstream of the cavity increases. Local heat transfer coefficient enhancement immediately downstream of the smallest hole (D/d = 2.5) is as high as 2.2, and it is as high as 4.5 for the largest cavity hole (D/d = 12.5). For a small cavity, the mainstream flow is trapped inside the cavity, producing low heat transfer ($h/h_0 <$ 1). Flow over a large cavity is similar to flow over a backstep, followed by forward-step at the downstream edge. Mainstream flow separates at the upstream edge and reattaches inside the cavity and is tripped by the downstream edge. Heat transfer is greatly enhanced at the cavity downstream because of the formation of a new boundary layer. Heat transfer inside

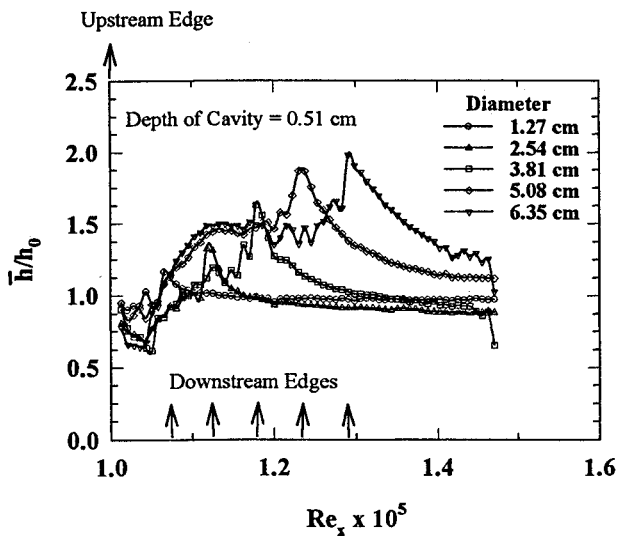

Fig. 5 Effect of cavity size on $\bar{h}/h_0$ distributions.

the cavity is enhanced as the cavity size increases because of reattachment of flow.

Figure 5 shows the effect of cavity size on spanwise-averaged heat transfer coefficient ratios $\bar{h}/h_0$. The highest heat transfer coefficient ratio is obtained immediately downstream of the downstream edge of the cavity for all sizes. The highest $\bar{h}/h_0$ value increases as the cavity size increases. The $\bar{h}/h_0$ values inside the cavity show increases as the cavity size increases. For the largest cavity, the ratio is as high as 1.6 inside the cavity and 2.0 downstream of the cavity.

Effect of Cavity Depth

Effect of d is tested for a circular cavity of D of 3.81 cm. The depths tested were 0.254, 0.51, and 0.76 cm. Corresponding d/θ ratios are 2.65, 5.3, and 7.92. Figure 6 presents the local heat transfer coefficient enhancement distributions for the three cavity depths. As the depth of the cavity hole increases, the heat transfer coefficient enhancement increases downstream of the cavity. The flow is more turbulent near the leading edge of the cavity hole because of increasing depth. As the depth increases, the reattachment location inside the cavity moves towards the downstream edge of the cavity. High heat transfer coefficients are observed at the reattachment location. Increasing cavity depth causes more separation at the upstream leading edge of the cavity causing higher heat transfer coefficient at the downstream edge inside the cavity hole. Heat transfer coefficient is low near the upstream edge of the cavity because of recirculation caused by the separation.

Figure 7 shows the effect of depth on $\bar{h}/h_0$. An increase in depth of the cavity from 0.254 to 0.76 cm increases heat transfer coefficient enhancement. Increased cavity depth increases reattachment and separation at the edges of the cavity, and increases heat transfer coefficients inside and outside the cavity. The highest heat transfer coefficient ratio is obtained immediately downstream of the downstream edge of the cavity.

Effect of Cavity Shape

The effect of cavity shape is studied for five different shapes other than the circle. These five shapes are square, diamond, rectangle, spanwise (vertical) ellipse, and streamwise (horizontal) ellipse. The depth for each of the five shapes is 0.51 cm. The corresponding d/θ value is 5.3. Heat transfer coefficient ratio distributions for all shapes are presented in Fig. 8.

The effect of the square cavity is similar to a back-step and forward-step combination. Local heat transfer coefficient enhancement immediately downstream of the cavity is as high as 3.5. Heat transfer coefficient is enhanced one side-length downstream of the cavity. Heat transfer coefficients within the

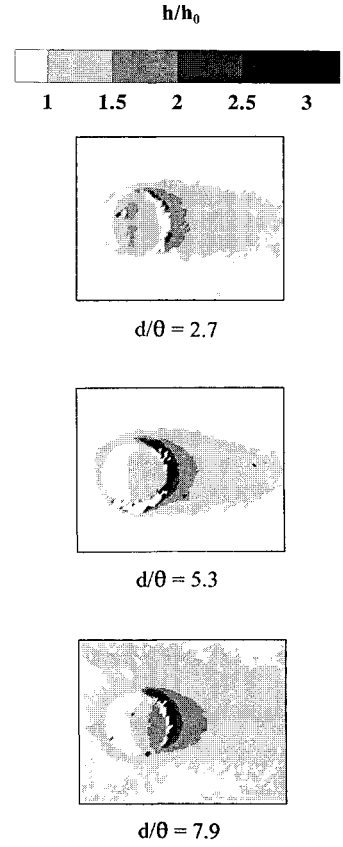

Fig. 6 Effect of cavity depth on local h/h_0 distributions.

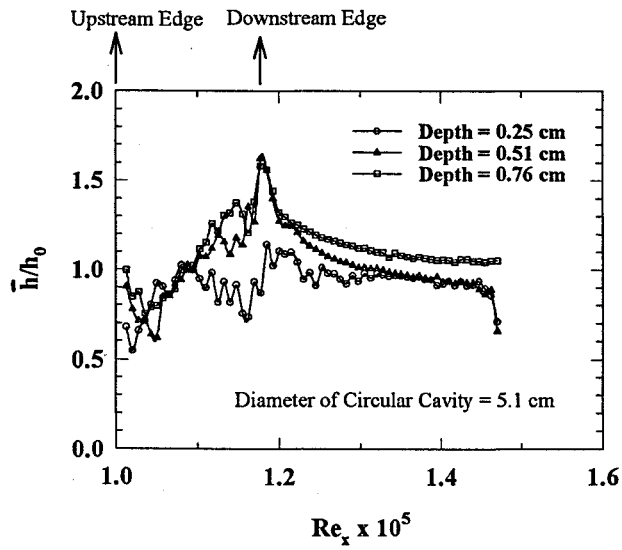

Fig. 7 Effect of cavity depth on $\bar{h}/h_0$ distributions.

cavity are also high because of reattachment of the mainstream following separation at the upstream edge.

The downstream sides of the diamond cavity trip the mainstream and increase heat transfer coefficients along those sides. Heat transfer coefficient enhancement is lower at the upstream and downstream inside tips because of the separation of flow along the edges. Heat transfer coefficients within the cavity are not as high as those for the square shape.

The rectangular cavity is not wide enough for the flow to reattach inside the cavity. Flow is tripped and the heat transfer coefficient is enhanced downstream of the cavity. The flow is similar to flow over a two-dimensional cavity. Heat transfer coefficient enhancement is lower compared with the square

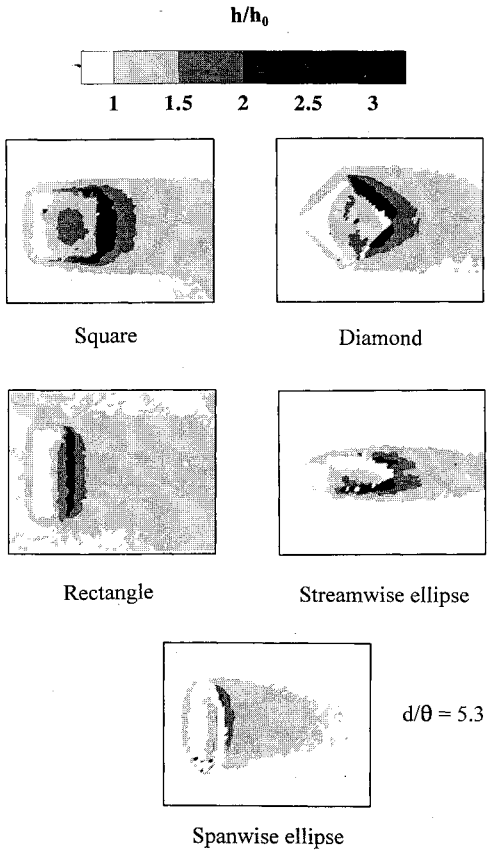

Fig. 8 Effect of cavity shape on local h/h_0 distributions.

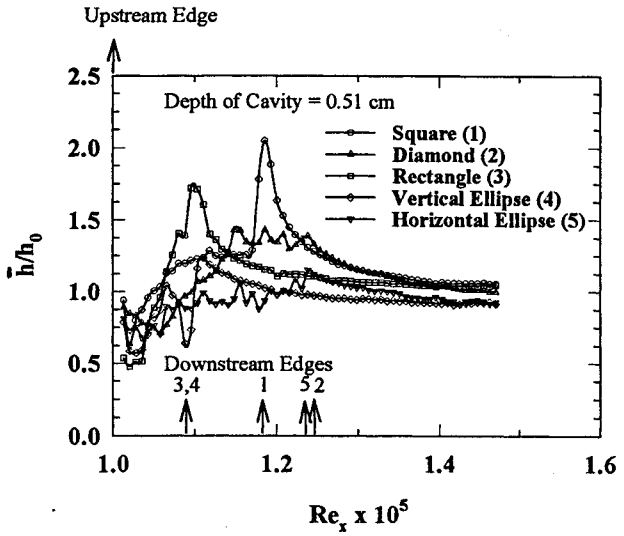

Fig. 9 Effect of cavity shape on $\bar{h}/h_0$ distributions.

cavity. Heat transfer coefficient enhancement is high immediately downstream of the cavity, but decreases rapidly downstream.

A streamwise ellipse produces longer enhanced regions downstream because of the length along the mainstream flow direction. Heat transfer coefficient enhancement is lower than for the other shapes and is limited to a small region along the upper and lower sides of the downstream edge. Heat transfer enhancement is also very low inside the cavity.

Heat transfer coefficient enhancement for the spanwise ellipse shape is the lowest compared with the other four shapes. The effect is small downstream of the cavity. Heat transfer coefficient enhancement within the cavity is also confined to a small region in the center of the cavity where the flow reattaches after separation at the upstream edge.

Figure 9 shows the effect of cavity shape on $\bar{h}/h_0$. Higher $\bar{h}/h_0$ values are obtained for a square, diamond, and the streamwise ellipse whose width along the flow is large. The enhancement is much lower for the spanwise ellipse. Heat transfer coefficient values are higher immediately downstream of the rectangular cavity, but decrease rapidly downstream. For larger widths along the flow, the disturbed boundary layer strongly increases heat transfer coefficient as for the square, diamond, and the horizontal ellipse. Ratios $\bar{h}/h_0$ inside the cavity are also higher for a cavity with a larger width along the flow.

Conclusions

The effect of cavity on heat transfer coefficients over a flat surface has been studied using a transient liquid crystal image method.

1) Detailed heat transfer coefficient distributions for various cavity depths, sizes, and shapes have been presented.

2) Heat transfer coefficient enhancement inside and downstream of the cavity increases with an increase of cavity size.

3) Downstream heat transfer coefficients are enhanced with an increase in depth of cavity on the entire surface. The reattachment location inside the cavity moves closer to the downstream edge with an increase in depth.

4) Heat transfer coefficient enhancement was obtained to be the highest for the square cavity. In general, cavities with longer axial length produced higher heat transfer enhancement on the surface.

Acknowledgments

This article was prepared with the support of the U.S. Department of Energy, Morgantown Energy Technology Center, Cooperative Agreement DE-FC21-92 MC 9061. The support of D. B. Fant and L. P. Golan, the technical team of Advanced Gas Turbine Systems Research at Clemson University, is greatly appreciated. The authors acknowledge C. Pang Lee, of General Electric Aircraft Engines, for his valuable suggestions on this project.

References

[1]Seban, R. A., "Heat Transfer and Flow in a Shallow Rectangular Cavity with Subsonic Turbulent Air Flow," *International Journal of Heat and Mass Transfer*, Vol. 8, No. 11, 1965, pp. 1353–1368.

[2]Yamamoto, H., Seki, N., and Fukusako, S., "Forced Convection Heat Transfer on Heated Bottom Surface of a Cavity," *Journal of Heat Transfer*, Vol. 101, No. 2, 1979, pp. 475–479.

[3]Chyu, M. K., and Goldstein, R. J., "Local Mass Transfer in Rectangular Cavities with Separated Turbulent Flow," 8th International Heat Transfer Conf., San Francisco, CA, 1986 (Paper 86-IHTC-230).

[4]Metzger, D. E., Bunker, R. S., and Chyu, M. K., "Cavity Heat Transfer on a Transverse Grooved Wall in a Narrow Flow Channel," *Journal of Heat Transfer*, Vol. 111, No. 1, 1989, pp. 73–79.

[5]Ireland, P. T., and Jones, T. V., "The Measurement of Local Heat Transfer Coefficients in Blade Cooling Geometries," *Conference on Heat Transfer and Cooling in Gas Turbines* (Bergen, Norway), CP 390, AGARD, 1985 (Paper 28).

[6]Clifford, R. J., Jones, T. V., and Dunne, S. T., "Techniques for Obtaining Detailed Heat Transfer Coefficient Measurements Within Gas Turbine Blade and Vane Cooling Passages," American Society of Mechanical Engineers Paper 83-GT-58, 1983.

[7]Metzger, D. E., and Larson, D. E., "Use of Melting Point Surface Coating for Local Convection Heat Transfer Measurements in Rectangular Channel Flows with 90° Turns," *Journal of Heat Transfer*, Vol. 108, No. 1, 1986, pp. 48–54.

[8]Hippensteele, S. A., Russell, L. M., and Stepka, F. S., "Evaluation of a Method for Heat Transfer Measurements and Thermal Visualization Using a Composite of a Heater Element and Liquid Crystals," *Journal of Heat Transfer*, Vol. 105, No. 1, 1983, pp. 184–189.

[9]Camci, C., Kim, K., and Hippensteele, S. A., "A New Hue Capturing Technique for the Quantitative Interpretation of Liquid Crystal Images Used in Convective Heat Transfer Studies," *Journal of Turbomachinery*, Vol. 114, No. 4, 1992, pp. 765–775.

[10]Baughn, J. W., and Yan, X., "An Insertion Technique Using the Transient Method with Liquid Crystals for Heat Transfer Measurement in Ducts," *Fouling and Enhancement Interactions*, American Society of Mechanical Engineers, HTD-Vol. 164, 1991, pp. 77–83.

[11]Hippensteele, S. A., and Poinsatte, P. E., "Transient Liquid Crystal Technique Used to Produce High-Resolution Convective Heat Transfer Coefficient Maps," *Visualization of Heat Transfer Processes*, American Society of Mechanical Engineers, HTD-Vol. 252, 1993, pp. 13–21.

[12]Camci, C., Kim, K., Hippensteele, S. A., and Poinsatte, P. E., "Evaluation of a Hue Capturing Based Transient Liquid Crystal Method for High-Resolution Mapping of Convective Heat Transfer on Curved Surfaces," *Journal of Heat Transfer*, Vol. 115, No. 2, 1993, pp. 311–318.

[13]Wang, Z., Ireland, P. T., and Jones, T. V., "An Advanced Method of Processing Liquid Crystal Video Signals from Heat Transfer Experiments," *Journal of Turbomachinery*, Vol. 117, No. 1, 1995, pp. 184–189.

[14]Ekkad, S. V., and Han, J. C., "Local Heat Transfer Distributions near a Sharp 180° Turn of a Two-Pass Smooth Square Channel Using a Transient Liquid Crystal Image Technique," *Journal of Flow Visualization and Image Processing*, Vol. 2, No. 3, 1995, pp. 184–189.

[15]Vedula, R. J., Metzger, D. E., and Bickford, W. B., "Effects of Lateral and Anisotropic Conduction on the Determination of Local Convection Heat Transfer Characteristics with Transient Tests and Surface Coating," *Collected Papers in Heat Transfer*, American Society of Mechanical Engineers, HTD-Vol. 104, 1988, pp. 21–28.

[16]Ireland, P. T., and Jones, T. V., "The Response Time of a Surface Thermometer Employing Encapsulated Thermochromic Liquid Crystals," *Journal of Physics E*, Vol. 20, Oct. 1987, pp. 1195–1199.

[17]Kline, S. J., and McClintock, F. A., "Describing Uncertainties in Single Sample Experiments," *Mechanical Engineering*, Vol. 75, Jan. 1953, pp. 3–8.